ULTRA SONO GRAPHY

Ultrasound biomicroscopy for the assessment of early-stage nonalcoholic fatty liver disease induced in rats by a high-fat diet

Antonio Carlos Soares Pantaleão Jr.[1], Marcio Pinto de Castro[2], Krishynan Shanty Fernandes Meirelles Araujo[3], Carlos Frederico Ferreira Campos[4], André Luiz Alves da Silva[1], José Eduardo Ferreira Manso[1], João Carlos Machado[1,5]

[1]Post-graduate Program in Surgical Sciences, Department of Surgery, School of Medicine, Federal University of Rio de Janeiro, Rio de Janeiro; [2]Veterinary Diagnostic Center (CEVET), Niterói; [3]Department of Electronics Engineering and Computing, Federal University of Rio de Janeiro, Rio de Janeiro; [4]Department of Pathology and Laboratories, University of the State of Rio de Janeiro, Rio de Janeiro; [5]Biomedical Engineering Program-COPPE/Federal University of Rio de Janeiro, Rio de Janeiro, Brazil

Purpose: The aim of this study was to assess the ability of ultrasound biomicroscopy (UBM) to diagnose the initial stages of nonalcoholic fatty liver disease (NAFLD) in a rat model.

Methods: Eighteen male Wistar rats were allocated to control or experimental groups. A high-fat diet (HFD) with 20% fructose and 2% cholesterol, resembling a common Western diet, was fed to animals in the experimental groups for up to 16 weeks; those in the control group received a regular diet. A 21 MHz UBM system was used to acquire B-mode images at specific times: baseline (T_0), 10 weeks (T_{10}), and 16 weeks (T_{16}). The sonographic hepatorenal index (SHRI), based on the average ultrasound image gray-level intensities from the liver parenchyma and right renal cortex, was determined at T_0, T_{10}, and T_{16}. The liver specimen histology was classified using the modified Nonalcoholic Steatohepatitis Clinical Research Network NAFLD activity scoring system.

Results: The livers in the animals in the experimental groups progressed from sinusoidal congestion and moderate macro- and micro-vesicular steatosis to moderate steatosis and frequent hepatocyte ballooning. The SHRI obtained in the experimental group animals at T_{10} and T_{16} was significantly different from the SHRI of pooled control group. No significant difference existed between the SHRI in animals receiving HFD between T_{10} and T_{16}.

Conclusion: SHRI measurement using UBM may be a promising noninvasive tool to characterize early-stage NAFLD in rat models.

Keywords: Nonalcoholic fatty liver disease; Animal models; High-fat diet; Dietary cholesterol; Ultrasonography

Key points: An animal model for nonalcoholic fatty liver disease (NAFLD) was developed based on a frequently used high fat Western diet consisting of 20% fructose and 2% cholesterol. NAFLD was diagnosed in the initial stages. The hepatorenal sonographic index was determined at three points along a timeline extending up to 16 weeks.

ORIGINAL ARTICLE

https://doi.org/10.14366/usg.21182
pISSN: 2288-5919 • eISSN: 2288-5943
Ultrasonography 2022;41:750-760

Received: August 31, 2021
Revised: February 19, 2022
Accepted: March 24, 2022

Correspondence to:
Antonio Carlos Soares Pantaleão Jr., MD, Post-graduate Program in Surgical Sciences, Department of Surgery, School of Medicine, Federal University of Rio de Janeiro, Hospital Universitário Clementino Fraga Filho, 11th floor, Block F, 255 Prof. Rodolpho Paulo Rocco St, Ilha do Fundão, Rio de Janeiro, RJ, ZIP 21941-617, Brazil
Tel. +55-21-26094713
Fax. +55-21-2710729
E-mail: acpantajunior@gmail.com

How to cite this article:
Pantaleão Jr. ACS, de Castro MP, Araujo KSFM, Campos CFF, da Silva ALA, Manso JEF, et al. Ultrasound biomicroscopy for the assessment of early-stage nonalcoholic fatty liver disease induced in rats by a high-fat diet. Ultrasonography. 2022 Oct;41(4):750-760.

Introduction

Obesity, a widespread disease throughout the world, has reached epidemic proportions; its age-standardized prevalence among adults (18 years and older) has increased globally by 1.5 times since 2000, and its crude prevalence in children (5–19 years) has more than doubled between 2000 and 2016 [1]. Obesity promotes an increased risk of heart disease, diabetes, depression, and many cancers, as well as premature death [2]. The global increase in obesity has been accompanied by an increase in nonalcoholic fatty liver disease (NAFLD), which refers to fat accumulation in the liver without excessive alcohol consumption and represents the hepatic manifestation of metabolic syndrome based on the consistent association between NAFLD and hypertension, dyslipidemia, insulin resistance, type 2 diabetes, and visceral adiposity [3]. Moreover, obesity and type 2 diabetes are strong risk factors for NAFLD [4].

The global pooled NAFLD prevalence is 25.24%, with wide geographical variation [5], and this prevalence ranges between 42.6% and 69.5% in patients affected by type 2 diabetes mellitus [6]. These epidemiological indicators show that NAFLD is a growing public health problem. Nonalcoholic steatohepatitis (NASH) represents its most severe form, resulting in chronic liver disease, liver cirrhosis, and hepatocellular carcinoma [7]. According to Schattenberg et al. [8], the prompt diagnosis and care of NASH patients will likely reduce future healthcare costs.

As discussed by Perumpail et al. [9], the increased prevalence of NAFLD poses challenges to healthcare systems regarding how to screen for the progressing epidemic of liver disease. Efforts to address these challenges should focus on understanding NAFLD pathophysiology and its treatment, which requires new diagnostic tools and methods to complement the diagnostic tests already employed, including liver biopsy as the gold standard, serum biomarkers and biomarker panels [10] and noninvasive imaging techniques such as hepatic ultrasonography [11], computed tomography, and magnetic resonance imaging [10]. NAFLD and NASH experimental models are also important elements of translational science in order to identify targets for diagnosis, monitoring, therapy, and histopathological outcomes in advance of costly clinical research [12]. Animal models have been used to investigate NAFLD and NASH [12–15], including C57BL/6 mice. Wistar and Sprague-Dawley rats are usually preferred due to their predilection to develop obesity, type 2 diabetes, NAFLD, and NASH [16,17].

In translational studies, animal models based on diet-induced NAFLD paralleling human dietary habits are predominant; these diets include a high-fat diet (HFD) and fructose [14,18], a monosaccharide primarily metabolized in the liver [18] and excessively consumed in Western societies. An HFD has between 45% and 75% of the kilocalories allocated to lipids and promotes a rat phenotype that is similar to human obesity, insulin resistance, glucose intolerance, and dyslipidemia. When a diet contains high levels of fat, cholesterol, and fructose, NAFLD progresses to NASH, and the three stages of NAFLD (steatosis, steatohepatitis with fibrosis, and cirrhosis) develop [19].

Concurrent with the reported animal diet-based models for NAFLD and NASH, ultrasound imaging methods have been used to diagnose liver disease in animals. In addition to providing a noninvasive method, ultrasound imaging is an adequate tool for detecting liver steatosis, longitudinally analyzing liver fibrosis progression, and diagnosing hepatic cirrhosis. Ultrasonographic methods consider the echographic relationship between the liver and the renal cortex [20,21], tissue characterization based on the statistical properties of the gray-level image intensity [22], elastography [23], or the liver parenchyma echotexture with [24] or without [25] the use of an ultrasound contrast agent. These ultrasound methods have been performed *in vivo* on rat models employing distinct approaches that did not mimic human dietary habits for diet-induced NAFLD. Furthermore, many of the aforementioned investigations based on rat models have evaluated hepatic impairment in its final stages.

The current work was conducted to diagnose the initial stages of NAFLD based on ultrasound biomicroscopy (UBM) images acquired *in vivo* from rats fed with HFD. The rationale for using UBM is that this technique uses ultrasonic frequencies higher than those typically employed in clinical ultrasonography to provide adequate spatial resolution to inspect small animals, with typical image resolutions of 30 μm (axial) and 72 μm (lateral) obtained using a 40 MHz UBM system [26]. The spatial resolution provided by high-frequency ultrasound provides more detailed images of tissue microstructure, at the expense of lower penetration in comparison with typically used frequencies in clinical ultrasonography. The backscattering decreases if the frequency is reduced and increases if the dimensions of the tissue microstructure are higher; and these compensating effects, in association with the spatial resolution, justify using high-frequency ultrasound in experiments with small animals and low-frequency ultrasound with human patients, considering the organs and microstructure dimensions in each situation.

The UBM images obtained in the current work were processed to generate the sonographic hepatorenal index (SHRI) [27], which was used for clinical quantification of liver steatosis and was calculated as the ratio between the average gray-level intensities of two regions of interest (ROI): one over the UBM image from liver parenchyma and another from the renal cortex [27]. The SHRI is a sensitive, reproducible, and operator-independent parameter used to quantify steatosis, even for small amounts of liver fat that

would likely be missed using conventional ultrasonography. In human patients, the index cutoff points to predict steatosis greater than 25% and 60% are 1.86 and 2.23, respectively [27]. With rats receiving diethylnitrosamine orally over the course of 12 weeks to induce hepatic fibrosis, the SHRI ranged from 0.25 (baseline) to 0.46 and 0.53 when determined at 10 and 13 weeks, respectively [28].

Materials and Methods

Compliance with Ethical Standards

The experiments were conducted in strict accordance with the recommendations in the Guide for the Care and Use of Laboratory Animals of the National Institute of Health. The local Ethics Committee for Animal Use in Research (CEUA) of the Biological Science Institute/Federal University of Rio de Janeiro approved the research protocol (061/19), which was prepared before the study and registered at CEUA. The Animal Research: Reporting of *In Vivo* Experiments (ARRIVE) guidelines were followed for the replacement, refinement, and reduction of animals. All the study data are available and maintained under the responsibility of the last author.

Study Design and Animals

Eighteen 2-month-old healthy male Wistar rats, *Rattus norvegicus*, from the Center of Experimental Surgery (Medical School from the Federal University of Rio de Janeiro, RJ, Brazil) and weighing between 250 and 300 g were selected from the vivarium, with female rats excluded because male sex is a predisposing factor for the development of NAFLD [16]. Each animal was anesthetized with 1.5% isoflurane in 1.5 L/min oxygen using a laboratory animal compact anesthesia system (Vevo Anesthesia System, VisualSonics, Toronto, Canada). The animals were marked for identification, and the identified animals were randomly assigned into four groups: control groups at 10 and 16 weeks, G_{CT10} (n=3) and G_{CT16} (n=3), respectively, and experimental groups at 10 and 16 weeks, G_{EP10} (n=6) and G_{EP16} (n=6), respectively. Animals in the same group were housed three per cage and maintained in a 12-hour light/dark cycle at 23°C. Food was offered ad libitum (25 g per animal per day). The animals in the G_{CT} group (animals from both G_{CT10} and G_{CT16}) received standard vivarium pelleted formula and water *ad libitum*, whereas those in G_{EP10} and G_{EP16} received an HFD rich in cholesterol and fructose for 10 and 16 weeks, respectively. The HFD (Table 1) was accompanied by water and a cola-based carbonated drink *ad libitum*. Adverse events for animals in G_{EP10} and G_{EP16} included diarrhea, which was more intense until the fifth week, when the signs started a gradual regression until complete disappearance at 8 weeks. The animals were weighed once a week in order to exclude any animal with significant weight loss.

The feeding periods of 10 and 16 weeks were selected based on the literatures [14,16], considering findings in mice fed an HFD. Ten weeks after receiving the HFD, the animals presented obesity, hyperlipidemia and hyperinsulinemia, and glucose intolerance after 12 weeks. Together, these signs represent a phenotype similar to the human disease [16]. Moreover, male C57BL/6 mice fed an HFD up to 16 weeks presented hepatic steatosis, hepatocyte ballooning, Mallory bodies, higher fasting serum glucose levels, and decreased adiponectin levels, suggesting hyperglycemia and insulin resistance [14]. Therefore, 16 weeks of feeding the animals with HFD seemed sufficient to promote lesions suggestive of NASH.

UBM Image Acquisition

Prior to UBM image acquisition using the experimental facilities at CENABIO (National Center of Structural Biology and Bioimaging), the animals were anesthetized with 2% isoflurane in 1.5 L/min oxygen in the supine position over a heated platform for rats (AS-11550, VisualSonics) and underwent abdominal trichotomy. The images were acquired using a UBM machine (Vevo 2100, VisualSonics) operating with a 21 MHz probe (MS-250, VisualSonics) oriented to acquire B-mode images in the sagittal plane containing parts of the liver and the right kidney cortex. Standard ultrasound gel was used to couple the probe and the animal skin. Fig. 1 depicts a picture of the imaging setup.

A cineloop with 100 frames of B-mode images was acquired during each animal examination and stored. The UBM image

Table 1. Formulation of the HFD, rich in cholesterol and fructose, used to induce NAFLD in the rats

Component	Concentration (mass percentage)	kcal (%)
Corn starch[a)]	17.15	14.4
Albumin (egg white)[b)]	20.00	16.8
Dextrinized corn starch[a)]	7.00	5.9
Fructose[a)]	20.00	16.8
Soybean oil[c)]	1.80	3.4
Hydrogenated fat[c)]	22.00	41.6
Microcrystalline cellulose	5.00	0.0
Mineral mix AIN 93G	3.50	0.0
Vitamin mix AIN 93[a)]	1.00	0.8
L cystine[b)]	0.30	0.3
Choline bitartrate	0.25	0.0
Cholesterol	2.00	0.0
BHT	0.01	0.0

% kcal: [a)]carbohydrate=37.9, [b)]protein=17.1, [c)]lipid=45.0.
HFD, high-fat diet; NAFLD, nonalcoholic fatty liver disease; AIN, American Institute of Nutrition; BHT, butylated hydroxytoluene.

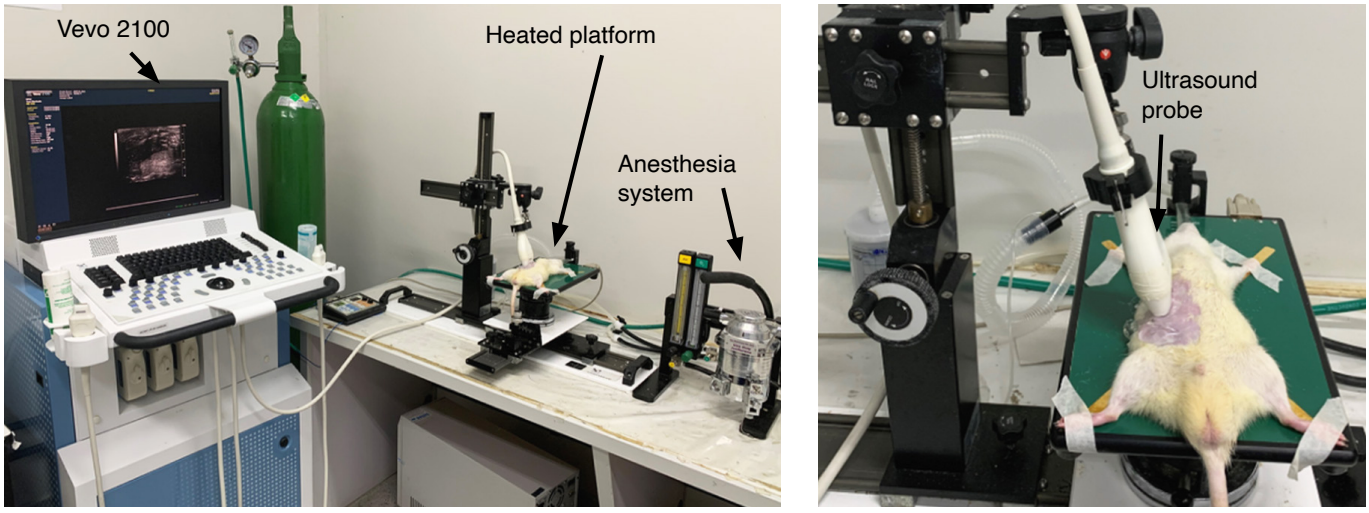

Fig. 1. Imaging setup.
A. Picture displaying the main devices used to acquire the ultrasound biomicroscopy images from the rat liver and kidney, including the Vevo 2100, the animal heated platform and the inhalatory anesthesia system. B. Detail of the ultrasound probe positioned over the rat abdomen.

acquisition timeline comprised three events, beginning with T_0, when all 18 animals had their images acquired and the animals in the G_{EP10} and G_{EP16} groups began the HFD. Ten weeks later (T_{10}), the animals in the G_{CT10} (n=3) and G_{EP10} (n=6) groups had their images acquired. Finally, the animals in the G_{CT16} (n=3) and G_{EP16} (n=6) groups had images acquired at T_{16} (16 weeks after T_0).

UBM Image Processing

The cineloop from each animal was inspected, supervised by an expert in ultrasound imaging of small animals, and three B-mode images (256 grayscale values) in the JPEG format were selected that contained views of the liver parenchyma and right renal cortex, with minor artifacts caused by respiratory or bowel motions. These three images were analyzed using the public domain Java image processing computational program ImageJ (version 1.47, NIH, Bethesda, MD, USA). The processing started with one ROI over the liver parenchyma and another over the renal cortex defined for each selected image. Each ROI was drawn based on the mouse pointer motion over the UBM selected image and using the LiveWire 2D tool, from ImageJ, to create the ROI closed contour. Subsequently, the mean gray-level intensities $AI_{L,i}$ and $AI_{K,i}$, ($1 \le i \le 3$), for each ROI over the liver parenchyma and renal cortex, respectively, were computed using the Measure tool from ImageJ. The SHRI was then calculated as $SHRI=(1/3)\cdot\sum_{i=1}^{3}(AI_{L,i}/AI_{K,i})$.

Histological Analysis

Following UBM image acquisition at T_{10} or T_{16}, the anesthetized animal was placed in a closed chamber saturated with isoflurane to induce euthanasia, and total hepatectomy was performed. The liver was weighed, fixed in a 10% neutral-buffered formalin solution, and sent *en bloc* to a single-blinded experienced hepatic pathologist that performed the cleavage in transverse sections encompassing all hepatic lobes, and produced 5-μm-thick sliced sections that were prepared for routine hematoxylin and eosin and picrosirius red staining. The hepatic pathologist evaluated all histological samples and graded them based on the modified version of the Nonalcoholic Steatohepatitis Clinical Research Network NAFLD activity scoring system [29], as shown in Table 2.

Table 2. Nonalcoholic Steatohepatitis Clinical Research Network NAFLD activity scoring system modified from the original version

Histological finding	Grades
Macro-steatosis	0 to 3
Portal inflammation	0 to 3
Lobular inflammation	0 to 3
Ballooning	0 to 2
Fibrosis	0 to 4

NAFLD, nonalcoholic fatty liver disease.

Statistical Analysis

Statistical tests were used to determine the sample size, the correlation coefficient between SHRI and animal weights, and significant differences among animal groups and for liver weights and the SHRI. The sample size, calculated based on the comparison of two means, used one-way analysis of variance (ANOVA) with

pairwise 2-sided tests and the following statistical coefficients: 0.8, 1.0, and 1.2 for the SHRI means of the G_{CT}, G_{EP10}, and G_{EP16} groups, respectively; 0.15 for the standard deviation; 3 for the number of comparisons between pairs; 0.80 for statistical power; and 0.05 as the level of significance. Further statistical analysis was performed using Jamovi software (version 1.1.9), a free and open-source statistical platform built on top of the R statistical language. Initially, the Shapiro-Wilk test for normality was employed, and if any group of experimental data was not normally distributed, then the nonparametric Kruskal-Wallis test followed by Dwass-Steel-Critchlow-Fligner pairwise comparisons was applied to determine whether the medians of the groups were significantly different. However, for all groups with normally distributed experimental data, the equality of the variances was determined, and one-way ANOVA was applied followed by the *post hoc* Tukey (equal variances) or Games-Howell (unequal variances) test to determine the significance of differences between the means of the groups. Values of $P<0.05$ (default) were considered to indicate statistical significance.

Results

Animal Weights

Plots of the mean (±standard deviation) of W_A/W_0, the animal weight W_A normalized by W_0 (weight at T_0), are presented for weeks 1 to 10 for the G_{CT10} and G_{EP10} groups and for weeks 1 to 16 for the G_{CT16} and G_{EP16} groups (Fig. 2). No significant weight loss occurred, and therefore no animal was excluded.

The W_A/W_0 results for the G_{CT10}, G_{CT16}, G_{EP10}, and G_{EP16} groups were not normally distributed; therefore, a nonparametric method was employed to compare the group weight medians. During weeks 1–10, there were no significant differences between the median values of W_A/W_0 for the G_{CT10} and G_{CT16} groups. However, the median values of W_A/W_0 of the G_{CT10} and G_{CT16} groups were significantly different from those of the G_{EP16} group. Furthermore, there were significant differences between the W_A/W_0 medians of the G_{CT10} and G_{CT16} groups and those of the G_{EP10} group after week 5. Finally, there were no significant differences between the median W_A/W_0 values of the G_{CT10} and G_{CT16} groups, except at weeks 5, 7, and 8. There was a significant difference between the W_A/W_0 median values between the G_{CT16} and G_{EP16} groups during weeks 11–16.

SHRI

A typical UBM image containing sections of the rat liver and right kidney is depicted in Fig. 3, including the ROIs used to calculate AI_L and AI_K. Both ROIs had similar depths to provide similar ultrasound attenuation effects of the wave incidence on the liver and kidney ROIs.

The Kruskal-Wallis test revealed no significant difference between the SHRI medians of the four groups determined on T_0 and the SHRI medians of the G_{CT10} group at T_{10} and the G_{CT16} group at T_{16}. Therefore, a group G_{CB} (n=24) was formed, pooling the SHRI results of the four groups determined at T_0 (n=18) with those for the G_{CT10} (n=3) and G_{CT16} (n=3) groups determined at T_{10} and T_{16}, respectively The Kruskal-Wallis test, followed by Dwass-Steel-Critchlow-Fligner pairwise comparisons, revealed a significant difference between

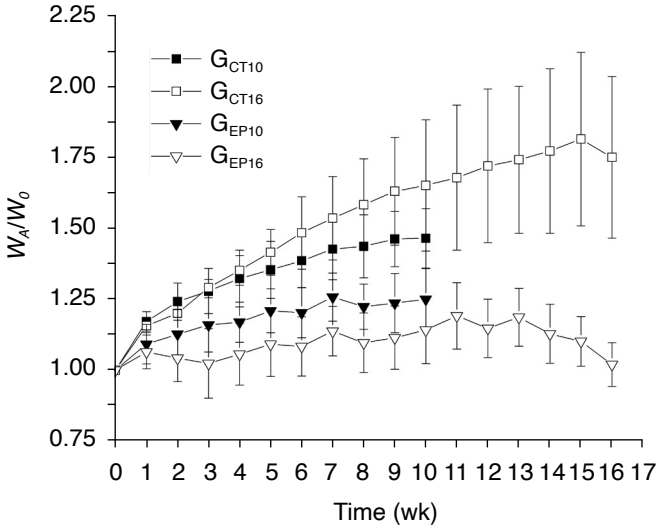

Fig. 2. **Weekly animal weights normalized to the weight at T_0.** Plots of the mean (±standard deviation) values for W_A/W_0, where W_A is the weekly weight and W_0 is the weight at T_0, for the animals in the G_{CT10}, G_{CT16}, G_{EP10}, and G_{EP16} groups during the feeding period of each group.

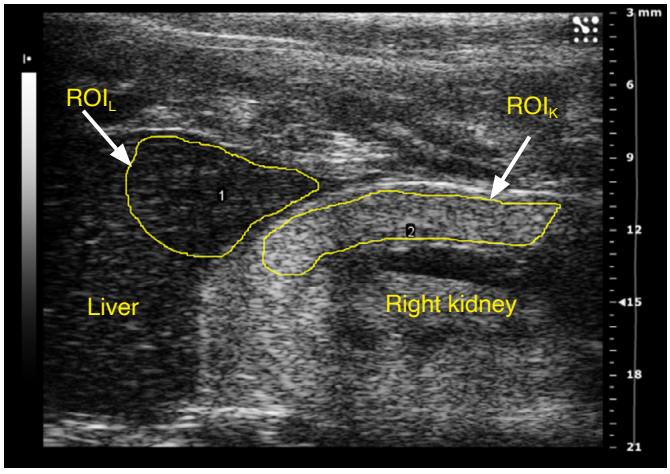

Fig. 3. **Typical 21-MHz ultrasound biomicroscopy image depicting sections of the rat liver and right kidney.** The regions of interest (ROI_L and ROI_K) surrounded by a yellow contour were used to calculate the corresponding the average gray-level intensities AI_L and AI_K for the liver and kidney parenchyma, respectively.

the median SHRI values of the G_{CB} and G_{EP10} groups and between the G_{CB} and G_{EP16} groups (P<0.05). No significant difference existed between G_{EP10} and G_{EP16} (P=0.183). A boxplot (Fig. 4) summarizes these results.

Liver Weight

The comparative macroscopic HFD effects on the liver are shown (Fig. 5) for one animal from $G_{CT,}$ one from G_{EP10} and one from G_{EP16}, euthanized at T_{16}, T_{10}, and T_{16}, respectively. The hepatic parenchyma of the animal in the G_{CT} group presented preserved macroscopic appearance, lobes with regular contours and a homogeneous brownish color. In contrast, the macroscopic changes in the liver of the animals from G_{EP10} and G_{EP16} presented heterogeneous coloration due to steatosis and vascular congestion. In addition, the liver of the rat from the G_{EP16} group had lobes with blunt edges.

The liver weights from animals in the G_{CT}, G_{EP10}, and G_{EP16} groups, either normalized to the corresponding animal weight measured just before euthanasia or in absolute values, were normally distributed. One-way ANOVA was then applied, followed by the Tukey *post hoc* test, and it was confirmed that the mean values of normalized liver weight showed significant (P<0.001) differences for G_{CT}×G_{EP10} and G_{EP10}×G_{EP16}, as well as for G_{CT}×G_{EP16} (P<0.01). The same *post hoc* test confirmed the absolute liver weights with significant (P<0.01) differences only for G_{CT}×G_{EP10} and G_{EP10}×G_{EP16}. The liver weights for all animals in each group are depicted in column plots in Fig. 6A and B for normalized and absolute values, respectively, and in boxplots in Fig. 6C and D for normalized and absolute values, respectively.

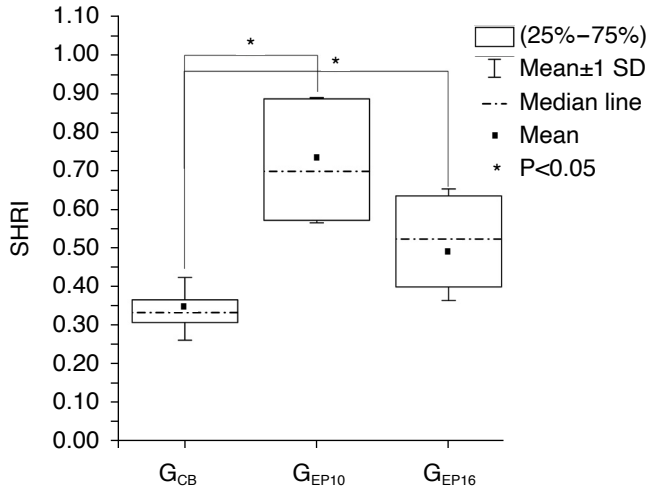

Fig. 4. Boxplot of the sonographic hepatorenal index (SHRI) measured on ultrasound biomicroscopy images of the liver and kidney parenchyma for animals in G_{CB}, G_{EP10}, and G_{EP16}. The median SHRI was significantly different (P<0.05) for G_{CB}×G_{EP10} and for G_{CB}×G_{EP16}. No significant difference was found between the SHRI results for the G_{EP10} and G_{EP16} groups. SD, standard deviation.

Histopathological Findings

Typical histological images of the livers of animals from the G_{CT10}, G_{EP10}, and G_{EP16} groups are presented (Fig. 7). The hepatic pathologist described the liver parenchyma of the animal in the G_{CT10} group as having a preserved architectural pattern, normal portal tract dimensions, and no inflammation. The same liver also showed an

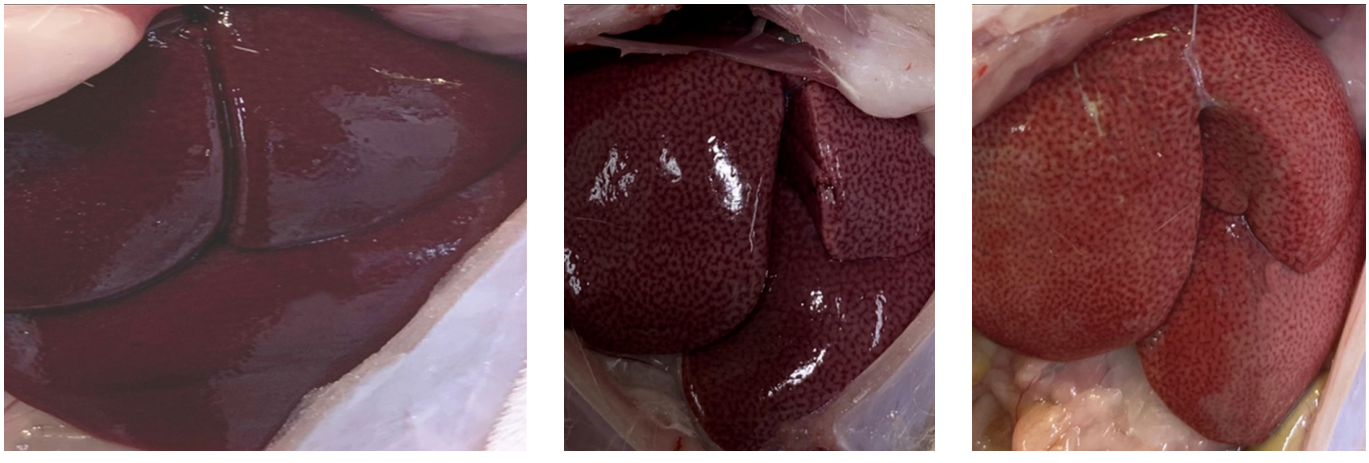

A B C

Fig. 5. Photographs of the rat liver immediately after euthanasia.
A. Animal from the control group euthanized at T_{16} with hepatic parenchyma shows a preserved macroscopic appearance, lobes with regular contours, and a homogeneous brownish color. B. Animal from the experimental group euthanized at T_{10} following administration of the high-fat diet (HFD) with macroscopic changes to the liver shows heterogeneous coloration due to steatosis and vascular congestion. C. Animal from the experimental group euthanized at T_{16} following administration of the HFD with macroscopic changes to the liver shows heterogeneous coloration due to steatosis and vascular congestion, as well as lobes with blunt edges.

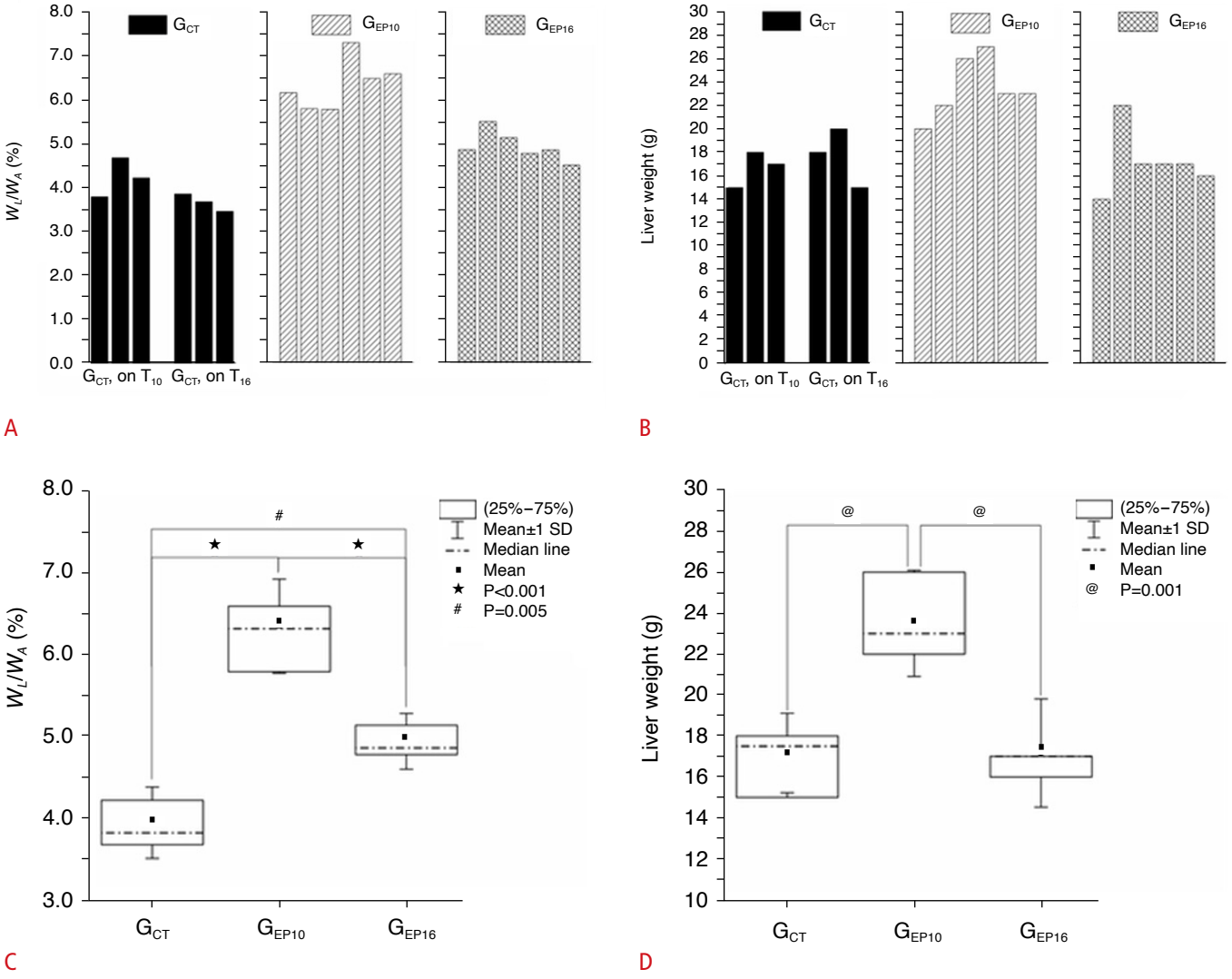

Fig. 6. Liver weights for animals in the G_{CT}, G_{EP10}, and G_{EP16} groups.
The liver weight, W_L, normalized to the animal weight, W_A, measured just prior to euthanasia, is depicted in column plots (A) and boxplots (C). Liver weights in absolute values are shown in column plots (B) and in boxplots (D). The mean normalized weights (%) were significantly different (P<0.001) for G_{CT}×G_{EP10} and G_{EP10}×G_{EP16} as well as for G_{CT}×G_{EP16} (P=0.005). The mean weights, in absolute values, were significantly different (P=0.001) only for G_{CT}×G_{EP10} and G_{EP10}×G_{EP16}. SD, standard deviation.

absence of steatosis and other significant histopathological changes in adjacent hepatocytes. Typical histological images of the liver from one animal of each group G_{CT10}, G_{EP10}, and G_{EP16} are presented (Fig. 7). The hepatic pathologist described the liver parenchyma of the particular animal in the G_{CT10} group having a preserved architectural pattern, normal portal tract dimensions, and no inflammation. The same liver also showed an absence of steatosis and other significant histopathological changes in adjacent hepatocytes. On the other hand, the specific animal in G_{EP10} group presented its liver parenchyma showing sinusoidal congestion and moderate macro- and micro-vesicular steatosis. Finally, the liver of the particular animal from the G_{EP16} group had sinusoidal congestion, moderate steatosis, and frequent hepatocyte ballooning.

The same hepatic pathologist graded the histological specimens of all 18 livers according to the activity scoring system defined in Table 2. The corresponding scores are shown in Table 3. None of the livers of animals in the G_{CT10} and G_{CT16} groups exhibited portal or lobular inflammation, ballooning, or fibrosis. Only one animal in the G_{CT10} group had a liver exhibiting macro-steatosis, which was graded with score 1. In contrast, five animals in the G_{EP10} group and three in the G_{EP16} group had liver macro-steatosis. In addition, five out of six (83.3%) of the animals in the G_{EP10} group had significant inflammatory activity characterized by occasional or frequent hepatocellular ballooning, which includes the presence of swollen

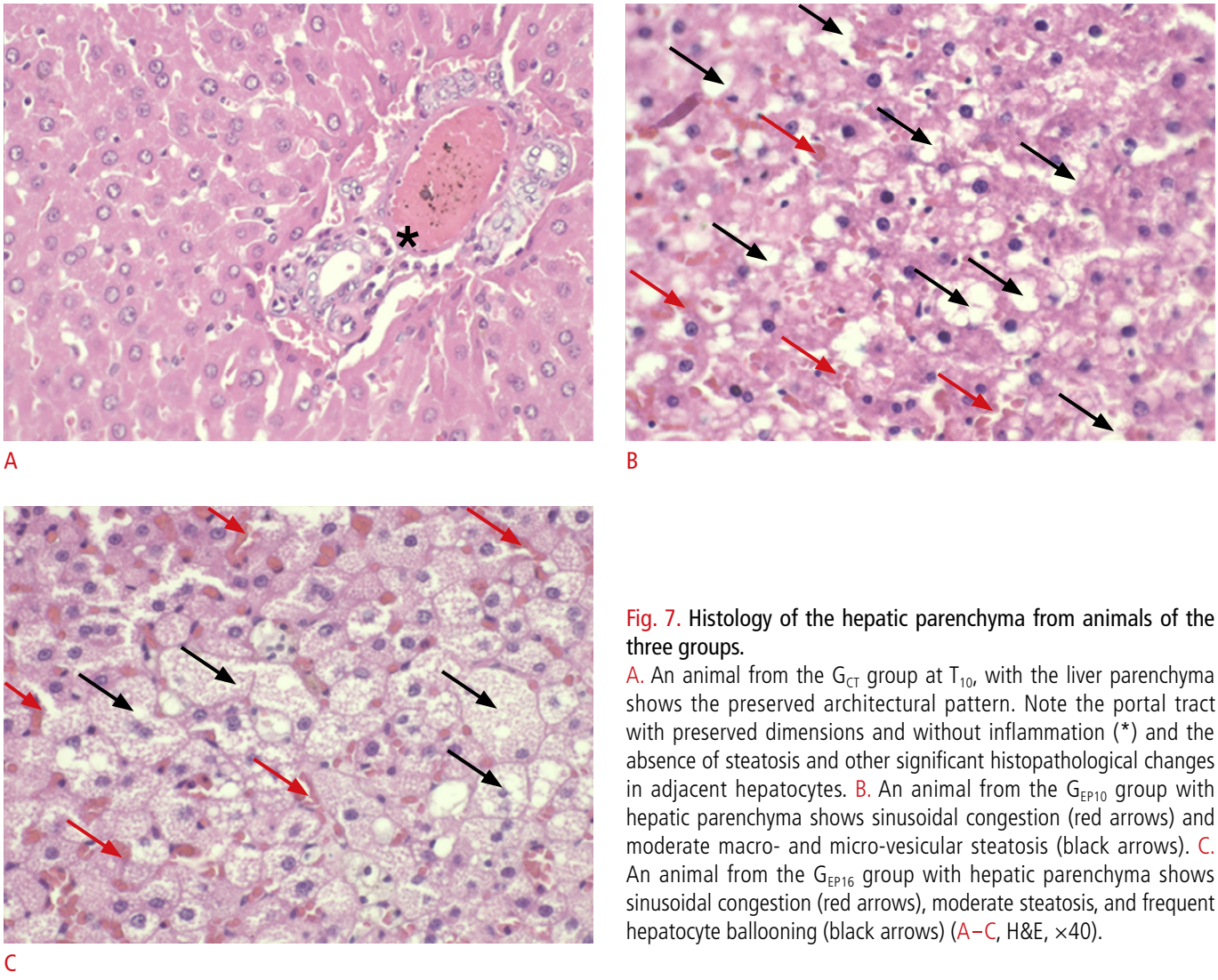

Fig. 7. Histology of the hepatic parenchyma from animals of the three groups.
A. An animal from the G_{CT} group at T_{10}, with the liver parenchyma shows the preserved architectural pattern. Note the portal tract with preserved dimensions and without inflammation (*) and the absence of steatosis and other significant histopathological changes in adjacent hepatocytes. B. An animal from the G_{EP10} group with hepatic parenchyma shows sinusoidal congestion (red arrows) and moderate macro- and micro-vesicular steatosis (black arrows). C. An animal from the G_{EP16} group with hepatic parenchyma shows sinusoidal congestion (red arrows), moderate steatosis, and frequent hepatocyte ballooning (black arrows) (A–C, H&E, ×40).

Table 3. Scores based on the activity scoring system defined in Table 2 according to the histological findings of the livers of all animals in each group

Histological finding	Scores for all animals in each animal group			
	G_{CT10} (n=3)	G_{CT16} (n=3)	G_{EP10} (n=6)	G_{EP16} (n=6)
Macro-steatosis	0, 1, 0	0, 0, 0	2, 1, 2, 0, 2, 2	0, 2, 0, 1, 0, 1
Portal inflammation	0, 0, 0	0, 0, 0	0, 0, 0, 0, 0, 0	0, 0, 0, 0, 0, 0
Lobular inflammation	0, 0, 0	0, 0, 0	0, 0, 0, 0, 1, 0	0, 1, 0, 0, 0, 0
Ballooning	0, 0, 0	0, 0, 0	1, 1, 1, 0, 2, 2	0, 2, 0, 1, 0, 2
Fibrosis	0, 0, 0	0, 0, 0	0, 0, 0, 0, 0, 0	0, 0, 0, 0, 0, 0

Scores occupying the same place on any line of the same column are linked to the same animal.

hepatocytes and rarefied cytoplasm, which may contain fat droplets and Mallory-Denk corpuscles, which usually represent a significant hepatocellular lesion [30]. Significant inflammatory activity occurred in 50% of animals in the G_{EP16} group. Lobular inflammation was present in one out of six (16.7%) of the animals in the G_{EP10} and G_{EP16} groups. Finally, no livers from animals in the G_{EP10} and G_{EP16} groups had portal inflammation or fibrosis.

Discussion

Hepatic fibrosis and cirrhosis represent the end stages of NAFLD, and the annual deaths from cirrhosis in the United States increased by 65% between 1999 and 2016 [31]. Consequently, diagnosing NAFLD/NASH in its early stages is important, as at these stages, there are still possible interventions that can dramatically modify the disease outcomes. Diagnostic and follow-up approaches that

are noninvasive, effective, and precise and have low-cost impacts on the general public health are necessary. In this context, Webb et al. [27] used ultrasonography as a promising tool, determining the SHRI to quantify liver steatosis in a clinical trial performed between 2005 and 2006. Subsequently, B-mode ultrasonography was used by Lessa et al. [20] to evaluate hepatic cirrhosis, and more recently, Tang et al. [23] combined quantitative ultrasonography and elastography with machine learning analysis to assess steatohepatitis, liver steatosis, inflammation, and fibrosis. Finally, D'Souza et al. [28] reported an assessment of hepatic fibrosis based on the SHRI. The aforementioned investigations, based on rat models, all evaluated hepatic impairment in its final stages and chemically induced hepatic diseases using a 20% solution of carbon tetrachloride [20], a methionine- and choline-deficient diet [23], or oral administration of diethylnitrosamine [28]. The methods reported previously have the limitation of inducing hepatic diseases that may not reflect concurrent liver diseases of varying etiologies. In contrast, the present work was conducted with liver disease induced by a diet typical of Western societies, consisting of the Amylin liver NASH model [19] modified by adding 5% more lipid calories and maintaining the concentrations of fructose (20%) and cholesterol (2%).

In the present work, the SHRI of the animals in the G_{EP10} and G_{EP16} groups increased and were significantly different from the SHRI of the animals in the G_{CB} group. The median SHRI for the G_{EP16} group was lower than the median SHRI for the G_{EP10} group, but there was no significant difference between them. It is worth noting (Fig. 2) that the mean normalized animal weight for the animal groups followed a trend similar to the one for the SHRI, with the mean normalized weight of the G_{EP16} group at T_{16} being lower than that of the G_{EP10} group at T_{10}. In this context, a positive Pearson correlation coefficient of 0.54 ($P<0.05$) was determined, indicating a moderate relationship between the normally distributed SHRI and the normalized weights for animals in the G_{EP10} group at T_{10}, and in the G_{EP16} group at T_{16}.

The work conducted by D'Souza et al. [28] and the present study employed similar methods and the same ultrasound frequency (21 MHz) to determine the SHRI, the values of which were similar between the control and experimental animal groups. Furthermore, the method employed to generate the SHRI is noninvasive and immune to variations in instrumentation settings used to optimize animal examinations, which is a relevant advantage of the method. The novelty of the present work in relation to the work reported by D'Souza et al. [28] relates, in essence, to the stage of the analyzed hepatic disease and to the animal model. While the current work imaged liver disease in its early stages and relied on an animal model based on diet-induced NAFLD paralleling human dietary habits, the work conducted by D'Souza et al. [28] inspected hepatic disease at an advanced stage, including liver fibrosis, and relied upon an animal model based on oral administration of diethylnitrosamine.

There was a weight increase in the animals in the control groups, whereas those receiving the HFD did not gain significant weight. The overall difference between animal weights normalized by the corresponding animal weight at T_0 for the control and experimental groups was significant after the fifth week. The literature presents conflicting results regarding weight changes in NAFLD animal models, as well as variation related to the length of the diet period, animals (strain, sex, and age), and the amount of calories allocated to fat [13]. Although some authors have reported that HFDs promote body weight increase, with physiological and phenotypical characteristics similar to human NAFLD [12,32,33], others did not report body weight differences between HFD and control groups [34–37]. Conversely, some studies reported weight decreases for animals in experimental groups [15,30,38] when employing diets with high-cholesterol concentrations, thus precluding the characteristic phenotype of obesity and metabolic syndrome. Moreover, the supplementation of a high-cholesterol and high-cholate diet with high-fat levels to animals can cause hepatic morphological alterations found in humans with NASH, as well as 9% body weight loss at the same time [18].

Although the animals in the present work receiving an HFD did not gain weight, their liver weight ratios did increase and normalized to the corresponding animal weight, did increase and the mean values were significantly higher ($P<0.01$) than that of the animals that did not receive an HFD (Fig. 6C). Additionally, the mean value of this ratio for the animals in the G_{EP10} group was higher ($P<0.001$) than in the animals in the G_{EP16} group; this should be explored in future works to determine whether the finding of less ballooning in animals from the G_{EP16} group is consistent with livers weighing less than those in animals from the G_{EP10} group. Regarding the liver weight in absolute values, only the animals in the G_{EP10} group presented a significant ($P<0.01$) difference in their mean liver weight in comparison with the corresponding results for the animals in the G_{CT} and G_{EP16} groups (Fig. 6D). As was observed for animal weight, the liver weight (normalized or not) followed a similar trend to that for the SHRI, with a relative increase at T_{10} in comparison to corresponding evaluations at T_0 and T_{16}.

As presented in Table 3, the animals in the G_{EP10} group exhibited more pronounced effects regarding macro-steatosis and ballooning than the animals in the G_{EP16} group, as expressed by the quantity of animals with scores greater than zero and with median scores of 2.0 and 0.5 for the G_{EP10} and G_{EP16} groups, respectively. For macro-steatosis, the corresponding median scores were 1.0 and 0.5. These findings should be explored in future works to determine whether

they can explain why the median SHRI of the G_{EP16} group was lower than that of the G_{EP10} group. From a histopathological point of view, the hallmark of NAFLD is hepatocellular steatosis, the presence of which is required in more than 5% of hepatocytes to diagnose this disease [30,39,40]. The histopathological findings in animals from the G_{EP10} and G_{EP16} groups are consistent with some of the NAFLD outcomes and include macro-steatosis, lobular inflammation and ballooning, with ballooning showing the highest scores. Despite the absence of the obesity and metabolic syndrome phenotype in the animals in this study fed an HFD, the histopathological findings enable the conclusion that the dietary model used herein effectively induced NAFLD and NASH in rats.

The findings in terms of animal and liver weights, as well as histopathology, provide important insights into the animal response to the HFD and the establishment of NAFLD and NASH. Furthermore, the current work concentrated on the ultrasonographic evaluation of NAFLD and NASH in their early stages in an animal model that relates more closely to translational fundamentals. The use of ultrasound imaging to image animal-induced hepatic disease, as introduced in the current work, establishes a basis for other investigations designed to diagnose NAFLD and NASH in animal models. The SHRI, based on a noninvasive method that is immune to variations in the instrumentation settings used to optimize animal examinations, represents a promising tool to characterize NAFLD in rat models.

ORCID: Antonio Carlos Soares Pantaleão Jr.: https://orcid.org/0000-0001-5992-9197; Marcio Pinto de Castro: https://orcid.org/0000-0003-3154-1988; Krishynan Shanty Fernandes Meirelles Araujo: https://orcid.org/0000-0001-6878-8402; Carlos Frederico Ferreira Campos: https://orcid.org/0000-0002-2623-1160; André Luiz Alves da Silva: https://orcid.org/0000-0002-0860-8067; José Eduardo Ferreira Manso: https://orcid.org/0000-0001-9694-7415; João Carlos Machado: https://orcid.org/0000-0003-2747-1702

Author Contributions

Conceptualization: Pantaleão Jr. ACS. Data acquisition: Pantaleão Jr. ACS, de Castro MP, da Silva ALA, Manso JEF, Machado JC. Data analysis or interpretation: Pantaleão Jr. ACS, Araujo KSFM, Campos CFF, Machado JC. Drafting of the manuscript: Pantaleão Jr. ACS, Manso JEF. Critical revision of the manuscript: Pantaleão Jr. ACS, de Castro MP, Araujo KSFM, Campos CFF, da Silva ALA, Machado JC. Approval of the final version of the manuscript: all authors.

Conflict of Interest

No potential conflict of interest relevant to this article was reported.

Acknowledgments

The authors thank CENABIO (National Center of Structural Biology and Bioimaging), from Federal University of Rio de Janeiro, for the care and handling of the animals and for allowing the use of the ultrasound image equipment. The authors thank Coordenação de Aperfeiçoamento de Pessoal de Nível Superior (CAPES) for financial support.

References

1. World Health Organization. World health statistics 2020: monitoring health for the SDGs, sustainable development goals. Geneva: World Health Organization, 2020.
2. Hruby A, Hu FB. The epidemiology of obesity: a big picture. Pharmacoeconomics 2015;33:673-689.
3. Tanaka N, Kimura T, Fujimori N, Nagaya T, Komatsu M, Tanaka E. Current status, problems, and perspectives of non-alcoholic fatty liver disease research. World J Gastroenterol 2019;25:163-177.
4. Wong VW, Chan WK, Chitturi S, Chawla Y, Dan YY, Duseja A, et al. Asia-Pacific Working Party on Non-alcoholic Fatty Liver Disease guidelines 2017-Part 1: definition, risk factors and assessment. J Gastroenterol Hepatol 2018;33:70-85.
5. Mitra S, De A, Chowdhury A. Epidemiology of non-alcoholic and alcoholic fatty liver diseases. Transl Gastroenterol Hepatol 2020;5:16.
6. Blachier M, Leleu H, Peck-Radosavljevic M, Valla DC, Roudot-Thoraval F. The burden of liver disease in Europe: a review of available epidemiological data. J Hepatol 2013;58:593-608.
7. Wong RJ, Aguilar M, Cheung R, Perumpail RB, Harrison SA, Younossi ZM, et al. Nonalcoholic steatohepatitis is the second leading etiology of liver disease among adults awaiting liver transplantation in the United States. Gastroenterology 2015;148:547-555.
8. Schattenberg JM, Lazarus JV, Newsome PN, Serfaty L, Aghemo A, Augustin S, et al. Disease burden and economic impact of diagnosed non-alcoholic steatohepatitis in five European countries in 2018: a cost-of-illness analysis. Liver Int 2021;41:1227-1242.
9. Perumpail BJ, Khan MA, Yoo ER, Cholankeril G, Kim D, Ahmed A. Clinical epidemiology and disease burden of nonalcoholic fatty liver disease. World J Gastroenterol 2017;23:8263-8276.
10. Zhou JH, Cai JJ, She ZG, Li HL. Noninvasive evaluation of nonalcoholic fatty liver disease: current evidence and practice. World J Gastroenterol 2019;25:1307-1326.
11. Jeon SK, Joo I, Kim SY, Jang JK, Park J, Park HS, et al. Quantitative ultrasound radiofrequency data analysis for the assessment of hepatic steatosis using the controlled attenuation parameter as a reference standard. Ultrasonography 2021;40:136-146.
12. Asgharpour A, Cazanave SC, Pacana T, Seneshaw M, Vincent R, Banini BA, et al. A diet-induced animal model of non-alcoholic fatty liver disease and hepatocellular cancer. J Hepatol 2016;65:579-588.
13. Kucera O, Cervinkova Z. Experimental models of non-alcoholic fatty

liver disease in rats. World J Gastroenterol 2014;20:8364-8376.
14. Lau JK, Zhang X, Yu J. Animal models of non-alcoholic fatty liver disease: current perspectives and recent advances. J Pathol 2017;241:36-44.
15. Zhang L, Wu X, Liao S, Li Y, Zhang Z, Chang Q, et al. Tree shrew (Tupaia belangeri chinensis), a novel non-obese animal model of non-alcoholic fatty liver disease. Biol Open 2016;5:1545-1552.
16. Van Herck MA, Vonghia L, Francque SM. Animal models of nonalcoholic fatty liver disease: a starter's guide. Nutrients 2017;9:1072.
17. Ichimura M, Kawase M, Masuzumi M, Sakaki M, Nagata Y, Tanaka K, et al. High-fat and high-cholesterol diet rapidly induces non-alcoholic steatohepatitis with advanced fibrosis in Sprague-Dawley rats. Hepatol Res 2015;45:458-469.
18. Sanches SC, Ramalho LN, Augusto MJ, da Silva DM, Ramalho FS. Nonalcoholic steatohepatitis: a search for factual animal models. Biomed Res Int 2015;2015:574832.
19. Kristiansen MN, Veidal SS, Rigbolt KT, Tolbol KS, Roth JD, Jelsing J, et al. Obese diet-induced mouse models of nonalcoholic steatohepatitis-tracking disease by liver biopsy. World J Hepatol 2016;8:673-684.
20. Lessa AS, Paredes BD, Dias JV, Carvalho AB, Quintanilha LF, Takiya CM, et al. Ultrasound imaging in an experimental model of fatty liver disease and cirrhosis in rats. BMC Vet Res 2010;6:6.
21. Turkay R, Aydin AF, Bingul I, Kucukgergin C, Dogan-Ekici I, Hocaoglu E, et al. Can ultrasound imaging predict the success of an experimental steatofibrosis model? Ultrasound Q 2017;33:157-161.
22. Zhou Z, Fang J, Cristea A, Lin YH, Tsai YW, Wan YL, et al. Value of homodyned K distribution in ultrasound parametric imaging of hepatic steatosis: an animal study. Ultrasonics 2020;101:106001.
23. Tang A, Destrempes F, Kazemirad S, Garcia-Duitama J, Nguyen BN, Cloutier G. Quantitative ultrasound and machine learning for assessment of steatohepatitis in a rat model. Eur Radiol 2019;29:2175-2184.
24. Miyata Y, Miyahara T, Moriyasu F. Decreased accumulation of ultrasound contrast in the liver of nonalcoholic steatohepatitis rat model. World J Gastroenterol 2011;17:4191-4198.
25. Chen W, Chen JY, Tung YT, Chen HL, Kuo CW, Chuang CH, et al. High-frequency ultrasound imaging to evaluate liver fibrosis progression in rats and yi guan jian herbal therapeutic effects. Evid Based Complement Alternat Med 2013;2013:302325.
26. Foster FS, Pavlin CJ, Harasiewicz KA, Christopher DA, Turnbull DH. Advances in ultrasound biomicroscopy. Ultrasound Med Biol 2000;26:1-27.
27. Webb M, Yeshua H, Zelber-Sagi S, Santo E, Brazowski E, Halpern Z, et al. Diagnostic value of a computerized hepatorenal index for sonographic quantification of liver steatosis. AJR Am J Roentgenol 2009;192:909-914.
28. D'Souza JC, Sultan LR, Hunt SJ, Schultz SM, Brice AK, Wood AK, et al. B-mode ultrasound for the assessment of hepatic fibrosis: a quantitative multiparametric analysis for a radiomics approach. Sci Rep 2019;9:8708.
29. Kleiner DE, Brunt EM, Van Natta M, Behling C, Contos MJ, Cummings OW, et al. Design and validation of a histological scoring system for nonalcoholic fatty liver disease. Hepatology 2005;41:1313-1321.
30. Takahashi Y, Soejima Y, Fukusato T. Animal models of nonalcoholic fatty liver disease/nonalcoholic steatohepatitis. World J Gastroenterol 2012;18:2300-2308.
31. Tapper EB, Parikh ND. Mortality due to cirrhosis and liver cancer in the United States, 1999-2016: observational study. BMJ 2018;362:k2817.
32. Koppe SW, Elias M, Moseley RH, Green RM. Trans fat feeding results in higher serum alanine aminotransferase and increased insulin resistance compared with a standard murine high-fat diet. Am J Physiol Gastrointest Liver Physiol 2009;297:G378-G384.
33. Fakhoury-Sayegh N, Trak-Smayra V, Khazzaka A, Esseily F, Obeid O, Lahoud-Zouein M, et al. Characteristics of nonalcoholic fatty liver disease induced in wistar rats following four different diets. Nutr Res Pract 2015;9:350-357.
34. Charlton M, Krishnan A, Viker K, Sanderson S, Cazanave S, McConico A, et al. Fast food diet mouse: novel small animal model of NASH with ballooning, progressive fibrosis, and high physiological fidelity to the human condition. Am J Physiol Gastrointest Liver Physiol 2011;301:G825-G834.
35. Lieber CS, Leo MA, Mak KM, Xu Y, Cao Q, Ren C, et al. Model of nonalcoholic steatohepatitis. Am J Clin Nutr 2004;79:502-509.
36. Eccleston HB, Andringa KK, Betancourt AM, King AL, Mantena SK, Swain TM, et al. Chronic exposure to a high-fat diet induces hepatic steatosis, impairs nitric oxide bioavailability, and modifies the mitochondrial proteome in mice. Antioxid Redox Signal 2011;15:447-459.
37. Brandt A, Jin CJ, Nolte K, Sellmann C, Engstler AJ, Bergheim I. Short-term intake of a fructose-, fat- and cholesterol-rich diet causes hepatic steatosis in mice: effect of antibiotic treatment. Nutrients 2017;9:1013.
38. Matsuzawa N, Takamura T, Kurita S, Misu H, Ota T, Ando H, et al. Lipid-induced oxidative stress causes steatohepatitis in mice fed an atherogenic diet. Hepatology 2007;46:1392-1403.
39. Neuschwander-Tetri BA, Clark JM, Bass NM, Van Natta ML, Unalp-Arida A, Tonascia J, et al. Clinical, laboratory and histological associations in adults with nonalcoholic fatty liver disease. Hepatology 2010;52:913-924.
40. Yeh MM, Brunt EM. Pathology of nonalcoholic fatty liver disease. Am J Clin Pathol 2007;128:837-847.